The Influence of Moss Colonization and Biochar Application on Evaporation Losses and Surface Crack in Shallow Carbonate–Derived Laterite During Dry–Wet Cycles

Lulu Che
Guizhou University
Dongdong Liu (liudongdongcn@foxmail.com)
Guizhou University https://orcid.org/0000-0001-8834-9167
Dongli She
Hohai University

Research Article

Keywords: Carbonate-derived laterite, Moss colonization, Biochar application, Soil evaporation, Surface crack.

Posted Date: December 8th, 2021

DOI: https://doi.org/10.21203/rs.3.rs-1109021/v1

The influence of moss colonization and biochar application on evaporation losses and surface crack in shallow carbonate–derived laterite during dry–wet cycles

Che Lulu[1], Liu Dongdong[1*], She Dongli[2]

[1]College of Resource and Environmental Engineering, Key Laboratory of Karst Georesources and Environment, Ministry of Education, Guizhou University, Guiyang, 550025, China

[2]College of Agricultural Sciences and Engineering, Hohai University, Nanjing 210098, China

*Corresponding author. Liu Dongdong, Email: ddliu@gzu.edu.cn

Tel: 86+15185160228

11 **Abstract**

12 *Aims* Soil water deficit in karst mountain lands is becoming an issue of concern
13 owing to porous, fissured, and soluble nature of underlying karst bedrock. It is
14 important to identify feasible methods to facilitate soil water preservation in karst
15 mountainous lands. This study aims to seek the possibility of combined utilization of
16 moss colonization and biochar application to reduce evaporation losses in
17 carbonate-derived laterite.

18 *Methods* The treatments of the experiments at micro-lysimeter included four moss
19 spore amounts (0, 30, 60, and 90 $g \cdot m^{-2}$) and four biochar application levels (0, 100,
20 400, and 700 $g \cdot m^{-3}$). The dynamics of moss coverage, characteristics of soil surface
21 cracks and surface temperature field were identified. An empirical evaporation model
22 considering the interactive effects of moss colonization and biochar application was
23 proposed and assessed.

24 *Results* Moss colonization reduced significantly the ratio of soil desiccation cracks.
25 Relative cumulative evaporation decreased linearly with increasing moss coverage
26 under four biochar application levels. Biochar application reduced critical moss
27 coverage associated with inhibition of evaporation by 33.26%-44.34%. The empirical
28 evaporation model enabled the calculation of soil evaporation losses under moss
29 colonization and biochar application, with the R^2 values ranging from 0.94 to 0.99.

30 *Conclusions* Our result showed that the artificially cultivated moss, which was
31 induced by moss spores and biochar, decreased soil evaporation by reducing soil

surface cracks, increasing soil moisture and soil surface temperature.Moss colonization and biochar application has the potential to facilitate soil moisture conservation in karst mountain lands.

Keywords Carbonate-derived laterite; Moss colonization; Biochar application; Soil evaporation; Surface crack.

Introduction

The karst landform, which plays a significant role in water supply and consumption, covers approximately 10% of the Earth's land surface (Yang et al. 2017). It covers extensive parts of China (~3,440,000 km^2), especially in southwestern China. These lands are usually characterized by a surface–underground structure. This sieve-like structure enhance soil water loss, soil drought, and rocky desertification. Because of the unrestrained water loss and the low water storage capacity, flora in karst lands grow slowly and exposed soils are easily eroded, which accelerate soil drought and pose threats to the stability of local ecosystems (Yang et al. 2017). Since the 1980s, a large number of vegetation restoration projects have been implemented to control rocky desertification in degraded karst ecosystems (Li et al. 2018). Although the efforts of large-scale afforestation drives should be applauded, the high cost of afforestation in karst lands and the low stability of restored areas remain a challenge (Chen et al. 2019). It is, therefore, important to identify viable and sustainable methods to facilitate soil water preservation in karst lands.

Evaporation plays a critical role in the terrestrial hydrological cycle and impacts water resource management directly and significantly (Liu et al. 2016). In particular, a wide range of negative effects, such as unrestrained water losses, poor water retention, and low storage capacity, are triggered by cracks in the soil–epikarst zone, which considerably limits vegetation restoration in karst ecosystems (Zhou et al. 2012). Although the climate is humid with abundant precipitation in karst ecosystems, water

deficits and drought events happens frequently due to shallow soil layer and weak soil water storage capacity. Therefore, evaporation is a dominant water flux of karst ecosystems, reducing excess of evaporation losses to retain more available water. Furthermore, there is difficult to implement water conservation measures in large scale underground. Most studies focused on how to reduce water losses in shallow soil (Table 1). In these studies, the complex effects of typical additives on evaporation processes, surface crack, and soil temperature in shallow soils were quantified and discussed (Xiao et al. 2010; Kidron et al. 2012; Chamizo et al. 2012., Zribi et al. 2015; Wang et al. 2018; Ni et al. 2018; Jiang et al. 2018; Wang et al. 2019; Zhang et al. 2020; Li et al. 2021). The effects of different vegetation types on soil evaporation and water balance in karst ecosystems were investigated. For example, Zhang et al. (2018) found that soil evaporation in the forest–grass ecosystems was significantly higher than that in crop and grass ecosystems of subtropical humid karst lands. A study by Swaffer et al. (2015) confirmed that the restriction of invasive alien species of plants could slightly reduce soil water losses in karst *Pinus massoniana* plantations. Nevertheless, the roles of moss colonization or other biological modifiers in soil evaporation processes during the forward succession of karst ecosystems have received little attention. The contribution of moss colonization and biochar application to the restoration and reconstruction of degraded karst ecosystems should be investigated.

Greater number of scientists have realized that the moss crust plays an essential role in ecological restoration in a great variety of climate zones (Xiao et al. 2010; Yang et al. 2012; Xiao et al. 2016; Liu et al. 2020). Moss effectively improves soil structural stability and soil water holding capacity in extreme environments (such as rocky desertification areas and desertification areas (Chen et al. 2019; Xie et al. 2019). Gao et al. (2012) found that moss could improve soil structure to reduce soil erosion in desertification areas. Moss has remarkable effects on reserving soil water, and that plays an important role in pedogenesis in karst rocky desertification areas (Li et al. 2009). Recently, artificial moss colonization was confirmed as an effective method that provides incentives to soil stability, water-holding capacity, and land alleviated degradation (Antoninka et al. 2015; Xiao et al. 2015). Zhao et al. (2014) found that artificial biocrusts could be formed rapidly, i.e., within a short-term period, thus improving micro-environment of soil surface. However, Xiao et al. (2011) showed that artificial moss crust under low-stress conditions differed from the natural ones in shape and species composition, which likely accounted for differences in the functions of the biocrust. Functions of biocrust in the terrestrial hydrological cycle is a matter of long-standing debate. Biocrusts increased soil infiltration ability by significantly upgrading hydraulic conductivity and surface macro-porosity (Jiang et al. 2018). Biocrusts also observably reduced surface soil infiltration capability and impeded soil water infiltration under ponding conditions (Xiao et al. 2019). Moreover, several studies have reported that the role of biocrusts in soil evaporation depends on

99 species, soil characteristics, and climates. Biocrusts greatly influenced evaporation
100 process of sandy soil in the Loess Plateau but no significant effect on sandy loam soil
101 (Xiao et al. 2011). Liu et al. (2020) concluded that for carbonate-derived laterite, moss
102 crusts could inhibit significantly evaporation losses and increase soil surface
103 temperature. Whereas moss colonization might be an attempt to address the obvious
104 problems that we face in holding sufficient soil water for ecosystems in karst lands,
105 more needs to be done to reduce the detrimental impact soil drought would have on
106 the ecosystem.

107 Several studies have claimed that biochar is conducive to improving soil
108 structure and properties, absorbing pollution, and promoting soil water retention
109 (Wang et al. 2018; Lei et al. 2019). Biochar seems to be an ideal soil amendment.
110 Zhang et al. (2016) reported that the biochars decreased saturated hydraulic
111 conductivity of sandy soil but did not reduce evaporation losses in the soil itself.
112 Zhang et al. (2020) found that biochar addition (0.5%, 2%, 4%, 6%, and 10%)
113 decreased evaporation rate of low-plasticity clay. Biochar also has positive effects on
114 plant growth. There was sufficient evidence that biochar could significantly facilitate
115 the growth of *Abutilon theophrasti* and *Prunella* by alleviating the side effects of salt
116 stress (Thomas et al. 2013). The most positive benefits of biochar, however, were that
117 it can enhance biocrust formation on the sand soil surface in a dry climate (Meng et al.
118 2014). Few studies have focused, however, on the potential effects of biochar on moss
119 growth in karst ecosystems faced with water shortages.

In accordance with recent surveys, we assume that the combined utilization of moss colonization and biochar application should have favorable impacts on soil hydrology, which will impede rocky desertification and contribute to restoring and conserving fragile ecosystems. Therefore, we conducted a series of evaporation experiments to determine the effects of moss colonization and biochar application on evaporation losses of carbonate-derived laterite during six dry–wet cycles. This study aimed to (1) determine the effects of moss colonization and biochar application on evaporation losses, variations in the surface temperature field, and development of soil surface cracks; (2) unravel the complicated relationship between moss colonization and soil evaporation under biochar application; and (3) develop a soil evaporation model that considers the moss colonization and biochar application.

Materials and methods

Study area

The sampling site was located in a *Pinus massoniana* forest (26°26′59.72″–26°26′43.01″ N and 106°39′2.23″–106°39′18.85″ E) in western Huaxi District, Guiyang City, Guizhou Province, China (Fig. 1a). This site is characterized by a subtropical monsoon climate. The annual mean precipitation and potential evaporation are 1,185 and 830 mm, respectively. Rainfall mainly occurs between May and October. The annual mean temperature is 14.9 °C, with the highest mean temperature (23.4 °C) in summer and the lowest mean temperature (4.9 °C) in winter. The site is covered with mixed soils—mainly sedimentary red soil and yellow soil

(carbonate-derived laterite). The lithology is dominated by limestone and dolomite with typical karst characteristics. Soil thickness is highly heterogeneous and the soil is characterized by large areas of exposed rock. The soil thickness is only 3-10 cm in most areas with severe rocky desertification (Ding et al. 2019). The landscape of the test site accurately represents the karst mountainous landform during the vegetation restoration process. Soil basic properties were determined by standard soil test methods and are shown in Table 2. Because of the underlying epikarst zone and poor soil water holding capacity, soil water deficits may occur frequently. Moss landscape patches are becoming fragmented and their spatial distribution is becoming homogenized and isolated, with coverage ranging from 0.32 to 0.95 $kg \cdot m^{-2}$ (Liu et al. 2020). The main moss species is *Hypnum Hedw*, which has homomorphic branches and leaves (Fig. 1b).

Experimental setup

The evaporation experiments were conducted from October 1, 2019, to January 2, 2020, under dry–wet cycles in closed greenhouse in the Key Laboratory of Karst Geological Resources and Environment in Guizhou University. A sampled carbonate-derived laterite collected in August 2019 from the upper 20 cm layer of the study site were used in these experiments. The sampled soils were passed through a 2 mm sieve and mixed after being air-dried. The biochar materials were bought from Laboratory of LiZhe Environmental Technology and produced from pyrolysis pine (Pinus sylvestris) at 450 and 550 °C. Subsequently, the biochar materials were sieved

through a 2 mm sieve. The moss was artificially cultivated by mixing different amounts of spores with soil materials found on the soil surface. The species of moss spores was *Hypnum Hedw.,* produced from Cao Mu Ji Plant Research Center. The effects of moss colonization and biochar application on moss growth, soil evaporation, and development of soil crack in carbonate-derived laterite were evaluated using 16 treatments with different amounts of biochar and moss spores. The treatments included four moss spores (0, 30, 60, and 90 $g \cdot m^{-2}$) and four biochar applications (0, 100, 400, and 700 $g \cdot m^{-3}$). The bare soil (0 $g \cdot m^{-2}$ moss spores and 0 $g \cdot m^{-3}$ biochar) were regarded as the control. Three replicates were prepared for each treatment and, thus, a total of 48 microlysimeters (10 cm diameter,4 cm soil thickness, and free drainage at the bottom) were operated (Fig. 1c). The microlysimeter scale referenced to previous studies on shallow soil amelioration (Table 1). It should be noted that using a microlysimeters in this study not give a complete soil evaporation processes occurring under field conditions. However, this microlysimeter scale of study enables systematic studies to be carried out under controlled conditions that enable insights into the changes in soil evaporation process under dynamic of soil surface characteristic. The soil materials were firstly divided into two layers to pack into these microlysimeters and biochar materials were added into the middle of the microlysimeter as a layer (Meng et al. 2014). The dry bulk density of the soil-biochar in the microlysimeter was controlled at 1.3 $g \cdot cm^{-3}$. The moss spores were mixed with the soil materials and evenly seeded onto the microlysimeter surface. After that, these

183 microlysimeters were saturated from the bottom by capillary action (self-absorption
184 method) until the top surface of soil column got wet and soaked for 72h to ensure
185 saturation. Finally, the bottom of microlysimeter was sealed with polyvinyl chloride
186 film to prevent drainage.

187 Evaporation experiments took place over six dry–wet cycles (D–W1, DW–2, D–
188 W3, D–W4, D–W5 and D–W6) (Fig.1 c). During each dry–wet cycle, evaporation
189 lasted for 12 days and saturation lasted for 3 days. The air temperature and
190 atmospheric relative humidity in the greenhouse were automatically measured using a
191 temperature and humidity recorder (Testo 174H, Testo SE & Co. KGaA, Germany),
192 which recorded data every 10 minutes. Because this study was conducted in the
193 closed greenhouse, the influence of wind was negligible. The microlysimeters were
194 weighed at 12:00 h every 2 days with an electronic precision balance of 0.01 g.
195 Evaporation losses were determined by applying the differences between the masses
196 of the microlysimeter. Simultaneously, thermal radiation of the soil surface were
197 recorded using a thermal camera (Testo 865, Testo SE & Co. KGaA, Germany). Real
198 soil surface images were also recorded by a high pixel digital camera (Eos 850D, 24.1
199 million pixels, Japan) to monitor the development of moss coverage and soil surface
200 crack. The vertical distance between the camera and the soil surface was set at 0.2 m.
201 All experiments were carried out within 10 min to ensure the accuracy of the data.

202 The initial variables were the number of moss spores, the number of biochar
203 applications, and sampled soil properties. Various evaporation indicators were

204 determined, including cumulative evaporation (E_c, mm), cumulative evaporation of
205 bare soil (E_{c0}, mm), evaporation rate (E, mm·d^{-1}), relative cumulative evaporation
206 (E_c/E_{c0}, -), and mean soil water content (SWC_{mean}, g·g^{-1}). E_c was determined by the
207 total evaporation losses during the entire evaporation time. E was calculated as the
208 ratio of the cumulative evaporation to evaporation time. E_c/E_{c0} was calculated as the
209 ratio of cumulative evaporation to bare soil evaporation for each treatment. SWC_{mean}
210 was determined by the conservation of mass.

211 $$E_c = 10\frac{E_m}{\rho\pi r^2} \quad (1)$$

212 where E_c is the cumulative evaporation (mm), E_m is the total evaporation loss during a
213 given duration (g), ρ is the density of water (1.0 g·cm^{-3}), and r is the radius of the
214 microlysimeter (10.0 cm).

215 $$SWC_{mean} = \frac{S_m \times \theta + S_w - E_m}{S_m(1-\theta)} \quad (2)$$

216 where SWC_{mean} is the mean soil water content (g·g^{-1}), S_m is the initial soil mass (g), S_w
217 is the increased water mass when microlysimeter saturated (g), and θ is the initial
218 soil water content (0.15 g·g^{-1}).

219 Image processing

220 Information on the development of moss coverage and soil surface crack was
221 extracted from real surface images using a Python script. The image processing was
222 conducted in the following two parts.

223 **Part 1: Crack-recognition module.** The soil surface cracks were discriminated
224 using a method similar to that used in Wang et al. (2017). Initially, this script picked

and cropped the edge areas and reserved the soil areas by threshold image segmentation and edge recognition. Subsequently, all the source images were converted into grayscale images, which switched from color differences between soil and crack to pixel difference. Owing to the visible difference in grayscale between cracks and soil blocks, these grayscale images were segmented into binary images by an automatic threshold method, called the OTSU method, implemented in the software package, Python OpenCV. If the grayscale values of some areas were higher than the threshold value, these areas were judged as cracks and shifted to black. Conversely, those areas below the threshold value were voted as soil materials and changed to white. The optical threshold value was automatically determined. It must be noted that very few isolated black spots could not be distinguished owing to the microtopography of the soil surface. Eventually, threshold denoising and characterization of cracks were performed (Fig. S1a). Several crack parameters were determined (see Section 2.4).

Part 2: Moss recognition module. There were obvious color differences between moss and soil, and thus color segmentation was applied to extract the dynamics of moss coverage. First, the mean filtering method was used to enhance the moss pixels. Later, the color mode of the source images was converted to HSV mode by the cvtColor function in OpenCV. The converted pictures were handled with color gamut segmentation by the THRESH_BINARY function in OpenCV. If the gray values were higher than the threshold value, these areas were judged as soils and

246 shifted to black. These areas below the threshold value were regarded as moss and
247 changed to white. The optical threshold value was also automatically determined.
248 Because the moss surface was irregular, there were a few noise points after image
249 binarization and segmentation. Finally, mathematical morphology processing was
250 conducted to fill holes after image binarization and segmentation (Fig. S1b).

251 The temporal and spatial evolution of the surface temperature for different
252 treatments were determined from these images using the IRSoft 4.5 software. The
253 thermal images of soil surface were collected using a thermal camera (Testo 865,
254 Testo SE & Co. KGaA, Germany). The IRSoft 4.5 software was used to automatically
255 analyze a thermal image. These thermal images were, then, imported into IRSoft 4.5
256 software to calculate the average temperature of the surface temperature for different
257 treatments (Fig. S1c).

258 Soil surface cracks, moss coverage, and moss growth

259 The crack ratio (R_{cr}) was calculated to illustrate the crack dynamics during the
260 dry–wet cycles. The crack ratio was determined as the ratio of crack pixels to total
261 pixels in the binarization images (Tang et al. 2011b; Wang et al. 2017).

262 $$R_{cr} = \frac{P_{black}}{P_{total}} \times 100 \quad (3)$$

263 where R_{cr} is the crack ratio (%), P_{black} is the pixel of the cracks in the binarization
264 images (-), and P_{total} is the pixel of soil in binary images (-).

265 Moss coverage was used as an indicator to reveal the moss growth during the
266 experiment. Moss coverage (Mc) was defined as the ratio of moss pixels to the total

267 pixels.

268 $$M_c = \frac{P_{white}}{P_{total}} \times 100 \quad (4)$$

269 where Mc is moss coverage (%), P_{white} is pixels referring to moss in binary images (-),

270 and P_{total} is pixels representing soil surface areas in binary images (-).

271 A logistic growth model was built to unravel the dynamics of moss coverage

272 (Wu et al. 2020).

273 $$Mc = \frac{M}{[1+be^{(-kt)}]} \times 100 \quad (5)$$

274 where M is the upper limit to moss coverage ($cm^2 \cdot cm^{-2}$), b is the mutation time for

275 growth rate (day), k is the growth rate of moss ($cm^2 \cdot cm^{-2} \cdot day^{-1}$), and t is the growth

276 time (day).

277 Evaporation model considering the role of moss colonization

278 We used an empirical model to calculate the effects of moss colonization and

279 biochar application on evaporation of carbonate-derived laterite. The model focused

280 on the relationship between dynamics of moss coverage and soil evaporation in dry–

281 wet cycles. The empirical model consisted of two parts: moss coverage estimation,

282 and evaporation calculation. We introduced the logistic growth equation to

283 characterize the dynamics of moss coverage, which included three critical

284 parameters—moss growth rate (k, $cm^2 \cdot cm^{-2} \cdot day^{-1}$), time for mutation of growth rate (b,

285 day), and upper limit to moss coverage (M, $cm^2 \cdot cm^{-2}$). There was a significant linear

286 relationship between the value of E_c/E_{c0} and moss coverage M_c (see Section 3.4).

287 Based on the variation of this linear fitting relationship, the cumulative evaporation

288 was calculated as follows:

289 $$E = E_{c0}(aM_c + c) \quad (6)$$

290 where E is the predicted evaporation (mm), E_{c0} is the evaporation of bare soil (mm),
291 M_c is the moss coverage ($cm^2 \cdot cm^{-2}$), and a and c are empirical coefficients (-).

292 Data collected over the 88 days included evaporation for each treatment within
293 the given duration E_c, evaporation of bare soil E_{c0}, and moss coverage with each day
294 M_c. The data were applied to test the empirical model.

295 Data analysis

296 All statistical analyses were performed using Python version 3.6. Partial
297 correlation and ANOVA analyses were conducted using a significance level of 0.05
298 and 0.01, respectively. The partial correlation coefficient measured the degree of
299 association between the two variables, with the effects of a set of controlling variables
300 removed. Means were compared using the least significant difference determined by
301 one-way analysis of variance. Regression analysis was conducted to determine the
302 relationships between each variable, and the determination coefficient (R^2) and root
303 mean square error (RMSE) were used to evaluate the performance of the applied
304 regression equations. We used structural equation modeling (SEM) to separate the
305 effects of moss colonization and biochar application on evaporation of
306 carbonate-derived laterite. The SEM was conducted using AMOS 2.1 software.

Results

Dynamics of moss coverage

The moss coverage versus time under different biochar application (B0, B1, B2, and B3) and moss spores (M1, M2, and M3) during six dry–wet cycles was indicated in Fig. 2. The soil surface of the moss colonization treatments showed similar changing patterns in the moss growth during each dry–wet cycle. In particular, moss coverage considerably increased, but dramatically decreased after approximately 3 days of evaporation. Another notable finding is that the mean growth rate of moss in the first three dry–wet cycles (D–W1, D–W2, and D–W3) was higher than in the last two dry–wet cycles (D–W4 and D–W6) and, therefore, it appears that the dynamics of moss coverage were greatly affected by evaporation times and dry–wet cycles.

The logistic growth equation could estimate the dynamics of moss coverage, but there were some restrictions in explaining the wilt of moss under drought conditions (Table 3). The determination coefficients R^2 (dimensionless) ranged from 0.60 to 0.74 and the RMSE (dimensionless) values were between 0.02 and 0.16. The M values (upper limit to moss coverage) and k values (moss growth rate) increased with the initial amount of moss spores, but they were not affected by the biochar application for all treatments.

The initial amount of moss spores and soil water content significantly increased moss coverage with partial correlation coefficients (pr) of 0.64 and 0.48, respectively (Table 4). However, moss coverage significantly reduced with the increase of biochar

application (pr = -0.11, $P < 0.01$) and atmospheric relative humidity (pr = -0.33, $P < 0.01$). These results suggested that the initial amount of moss spores and soil water content had the largest impact on the growth of moss, whereas the biochar application had the lowest influence. These trends were also confirmed by the functional relationship among initial amount of moss spores, soil water content, air temperature, and atmospheric relative humidity ($M_c = 0.08 + 0.001M_b + 0.12SWC_{mean} - 0.04T_{air} - 0.01RH_{mean}$, $R^2 = 0.56$), where M_b is the initial amount of moss spores, SWC_{mean} is the mean soil water content during the drying process, T_{air} is the air temperature, and RH_{mean} is the mean atmospheric relative humidity.

Characteristics of soil surface cracks

The ratio of soil surface crack fluctuated significantly during dry–wet cycles. For example, the mean ratio of soil surface crack at the end of the D–W6 was 42.5% higher than that at the end of the D–W1 (Fig. 3). In each dry–wet cycle, there were significant differences in the mean soil surface crack ratio between different initial amounts of moss spores ($P < 0.05$), especially for the M3 treatment. In contrast, there were no significant differences in the mean soil surface crack ratio between different biochar applications ($P > 0.05$). The further fitting analysis showed that the mean ratio of soil surface crack declined linearly with an increase in the number of moss spores for the B0, B1, B2, and B3 treatments ($R^2 = 0.76$, 0.99, 0.25, and 0.59, respectively) (Fig. 4). The mean soil surface crack ratio increased linearly with an increase in the amount of biochar application for the M1 and M3 treatments ($R^2 = 0.25$ and 0.96,

349 respectively). Nevertheless, the mean ratio of soil surface crack was not influenced by
350 the biochar application for the M0 and M2 treatments (R^2 = 0.02 and 0.08,
351 respectively). It seems that the moss colonization significantly impeded the
352 development of soil surface cracks in most cases, but the effects of biochar
353 application on the development of soil surface cracks could not reach a clear
354 conclusion.

355 The above fitting results were slightly contradicted the results of the partial
356 correlation analysis. The partial correlation analysis indicated that the biochar
357 application and initial amounts of moss spores did not have significant effect on the
358 development of soil surface cracks (Table 4). This was mainly because the fitting
359 analysis did not considered the effects of moss coverage on the formation of soil
360 surface cracks (see Section 3.1). On the other hand, the ratio of soil surface crack
361 significantly decreased with an increase in the mean atmospheric relative humidity (pr
362 = -0.18, $P < 0.01$), but it significantly increased with an increase in the mean air
363 temperature (pr = 0.34, $P < 0.01$).

364 Relationship between growth of moss, soil water content and crack development

365 The ratio of soil surface crack increased significantly with the decreasing soil
366 water content (Fig. S2). The soil water content at the occurrence of cracking was
367 defined as critical water content (θ_c). The θ_c in the first dry–wet cycle (D–W1) does
368 not synchronize with that in the sixth dry–wet cycle (D–W6). For D–W1, θ_c varied in
369 the range of 39%-43%. On the other hand, θ_c ranged from 58% to 64% for all

treatments in D-W6. The most interesting discovery was that the moss growth could impede the formation of soil surface cracks for most dry–wet cycles, except for the first and fourth dry–wet cycles (D–W1 and D–W4) (Fig. 5). The main reason for the exceptions was that the moss coverage in D–W1 was too low to affect the formation of soil surface cracks, whereas the formation of soil surface cracks in D–W4 was inactive owing to the relatively low evaporation losses.

Soil evaporation process

Evaporation processes had gone through a constant rate stage and a falling rate stage in most dry–wet cycles (D–W1, D–W2, D–W3 and D–W5) (Table S1). The evaporation remained at a constant rate stage in D-W4 and D-W6 due to the decreasing atmospheric energy (Fig. S3). Despite the existence of moss colonization and biochar, the cumulative evaporation showed fitting relationships with evaporation time, and R^2 ranged from 0.77 to 0.97 (Table S1). For all dry-wet cycles, the lowest soil evaporation was observed in treatment with moss colonization and biochar application. For instance, the value of λ_1 for B1M1 treatment was the lowest in D–W1, D–W2 and D-W3, which were 5.87, 4.27 and 4.75, respectively. The value of λ_2 for B1M3 treatment was the lowest in D–W4 and D–W6, which were 0.66 and 0.88, respectively. These results showed that the moss colonization and the biochar application could reduce evaporation losses.

The relative cumulative evaporation E_c/E_{c0} (the ratio of cumulative evaporation E_c to cumulative evaporation of bare soil E_{c0}) was calculated to eliminate the

391 influence of the atmospheric condition. The dynamics of relative cumulative
392 evaporation for the M1, M2, and M3 treatments largely depended on the changes in
393 moss coverage (Fig. S4). For all treatments of moss colonization and biochar
394 application, the E_c/E_{c0} was significantly lower in D–W6 than D–W1, and the moss
395 coverage was significantly higher in early D–W6 than the initial moment of D–W1
396 (Fig. 6). In the other words, the moss colonization and biochar application over six
397 dry-wet cycles decreasing evaporation losses by 4.9%-28.3%. However, the effects of
398 moss colonization and biochar application on the relative cumulative evaporation
399 were hard to distinguish due to moss coverage was fluctuated in six dry-wet cycles.
400 The further fitting analysis indicated that moss colonization and biochar
401 application could decrease greatly evaporation losses. The fitting analyses showed
402 that the relative cumulative evaporation linearly decreased with an increase in moss
403 coverage for the B0, B1, B2, and B3 treatments (R^2 = 0.34, 0.44, 0.46, and 0.49,
404 respectively) (Fig. 7). The relative cumulative evaporation for different biochar
405 applications (B0, B1, B2, and B3) decreased with increasing moss coverage by
406 27.07%, 40.69%, 37.73%, and 31.37%, respectively. The relative cumulative
407 evaporation was 1 as the moss coverage reached a critical value. In other words, the
408 moss enhanced the evaporation losses when the moss coverage was below the critical
409 value, and reduced the evaporation losses when the moss developed to the critical
410 moss coverage. The critical moss coverage was 4.51%, 2.51%, 3.01%, and 0% for B0,
411 B1, B2 and B3 treatments, respectively. The critical moss coverage decreased with the

increasing biochar dosage even further to 0 percent. Partial correlation analyses indicated that the mean evaporation rate significantly increased with air temperature, the initial moss spore amount, and soil water content (pr = 0.42, 0.11, and 0.12, respectively) (Table 4). Moss coverage reduced significantly the mean evaporation rate with a partial correlation of -0.21. These results showed that the effects of moss colonization on evaporation losses were strengthened by the biochar application reduced critical moss coverage.

Surface temperature field

The comparison of the surface temperature during six dry–wet cycles under moss colonization and biochar application is shown in Fig. 8. The difference of surface temperature between moss cover and bare soil (T_{moss}-$T_{bare\text{-}soil}$) in the D–W1 are less than zero. Moss colonization with biochar application at D–W1 decreased the soil surface temperature by 0.21, 0.56, 0.48 and 0.55 ℃ respectively. The values of T_{moss} -$T_{bare\text{-}soil}$ became more than zero from D–W2 to D–W6 when the mature moss was observed. These results indicted that mature moss increased the soil surface temperature.

Partial correlation analyses indicated that the mean surface temperature significantly increased with increasing moss coverage (pr = 0.11 $P < 0.01$) and air temperature (pr = 0.43, $P < 0.01$). However, the mean surface temperature not significantly affected by the biochar application (pr = 0.01 $P > 0.05$) (Table 4). These results indicated that the of mature moss on the surface temperature significantly

increased the soil surface temperature, and the effects of the moss on the surface temperature were not largely affected by the biochar.

Evaporation estimation considering the role of moss colonization

Fig. 7 suggests that there was a linear relationship between E_c/E_{c0} and Mc. One variation in this relationship was to formulate an equation between Ec and Mc. Table 3 shows that the moss growth could be unraveled by a logistic growth equation. The combination of the two equations allows us to predict the effects of moss colonization on soil evaporation, and the model performances are shown in Table 3. The R^2 values ranged from 0.94 to 0.99, and the RMSE values varied between 0.16 and 0.43. These results showed that the combination of the two equations worked very well in 62.5% of all treatments with a low RMSE of less than 0.30. The combination of the two equations was an attempt to address the challenges in simulating the effects of moss growth on evaporation processes in carbonate-derived laterite. However, further work is needed to reduce the inaccuracy in the remaining 37.5% of treatments.

Discussion

Shifting relationships among moss colonization, biochar application, and soil evaporation

The effects of moss colonization and biochar application on the evaporation process of carbonate-derived laterite during the dry–wet cycles could originate from three important “dynamics”: (1) dynamics of moss coverage due to dry–wet cycles, (2)

453 dynamics of soil surface cracks owing to the influences of biochar application and
454 growth of moss, and (3) dynamics of surface temperature due to moss cover.

455 **Dynamics of moss coverage due to dry–wet cycles.** This study indicated that
456 the growth trend of artificially cultivated moss was classically vulnerable to dry–wet
457 cycles (Fig. 2). Moss coverage could reach only 25% after approximately 13 weeks
458 when the moss had suffered six dry–wet cycles. This result was very similar to the
459 conclusions by Antoninka et al. (2015). However, Zhao et al. (2014) showed that
460 moss coverage linearly increased in a well-hydrated greenhouse, and reached more
461 than 65% after only weeks. The main reason for the difference was probably that
462 moss colonization was largely restricted in serious water scarce conditions, and the
463 moss could reproduce very quickly under wetting conditions (Wei et al. 2010).
464 Another possible reason is that the artificial moss differed in shapes and species from
465 wild moss (Xiao et al. 2011), and thus the adaptation of artificial moss to the soil
466 water deficit was weaker than that of wild moss. What is new is the urgent need to
467 scale up this technology to accommodate the field scale, such as the field of rocky
468 desertification regions.

469 **Dynamics of soil surface cracks owing to the influences of biochar**
470 **application and moss growth.** Moss coverage reduced significantly soil surface
471 cracks (Figs. 4 and 6). Moss crusts significantly enhanced the water retention
472 characteristics in shallow soils (Mager et al. 2011; Chamizo et al. 2012; Xiao et al.
473 2016), which probably restrained the development of soil surface cracks. Although

biochar application had no direct influence on soil surface crack development, and biochar could inhibit slightly the growth of moss during the dry–wet cycles (Fig. 2 and 3). Normally, difference in matrix potential among soil materials leads to the development of cracks on the soil surface (Chen et al. 2019). Biochar in soil materials can change the soil cohesive power to affect the desiccation cracking characteristics of clay (Zhang et al. 2020). The development of soil surface cracks has several negative impacts, such as threatening soil stability and facilitating evaporation and infiltration (Wan et al. 2019; Poulsen, et al. 2020). However, unexpectedly, our results showed that the biochar played no direct role in soil surface crack under moss cover (Table 4). This may be due to the moss affected swelling–shrinkage characteristics of carbonate-derived laterite. The effects of the swelling–shrinkage on the development of soil surface cracks outperformed those of biochar applications (Zong et al. 2014; Zhang et al. 2020).

Dynamics of surface temperature due to moss cover. The mature moss had a considerable heat preservation effect on carbonate-derived laterite, which was indicated by the clear differences in surface temperature between soil and moss (T_{moss} -$T_{bare\ soil}$) (Fig. 8). This result was consistent with our previous finding, that moss crusts could increase the surface temperature of soil column by changing the soil surface reflectivity (Liu et al. 2020). However, this result was different from the results reported by Xiao et al. (2016), that moss crust could reduce significantly the underlying soil temperature by up to 11.8 °C in summer in semi-arid regions. The

most likely reason for this is that the moss was able to adapt to the diurnal temperature variations for survival. Another possible reason was that moss coverage increased the soil water content during the dry–wet cycles ($pr = 0.48$, $P < 0.01$) (Table 4). The moss crust can reserve soil water, and soil water can delay the decrease in soil temperature (Kidron et al. 2012; Chamizo et al.2013). As the soil evaporates, the soil layer becomes dry, and water in the soil becomes a prime factor affecting the soil temperature (Liu et al. 2020).

In response to this, we drew a mind map of the effects of moss colonization and biochar application on the evaporation losses of carbonate-derived laterite, and constructed a SEM based on the mind map and partial correlation analyses (Fig. 9). Moss colonization and biochar application played an important role in evaporation processes in three primary ways. First, the increase of initial amount of moss spores promotes the growth of moss ($pr = 0.64$, $P < 0.01$), but biochar application reduced slightly moss coverage ($pr = -0.11$, $P < 0.01$). Second, moss covers promoted the development of soil surface cracks ($pr = -0.13$, $P < 0.05$), and the increasing soil surface cracks enhanced evaporation losses ($pr = 0.32$, $P < 0.01$). Moreover, the moss decreased evaporation losses by reserving soil water content ($pr = 0.47$, $P < 0.05$), and the increasing soil water underlying the moss layer decreased evaporation losses ($pr = -0.21$, $P < 0.05$). Finally, the moss increased soil surface temperature ($pr = 0.11$, $P < 0.01$), and the increasing soil surface temperature enhanced evaporation loss ($pr = 0.28$, $P < 0.01$). In addition, our SEM explained 71% of variation in soil evaporation

under moss colonization and biochar application. Moss spores (standardized coefficients = 0.48, $P < 0.001$) and soil water content (standardized coefficients = 0.6, $P < 0.001$) had positive effects on moss growth. Atmospheric humidity (standardized coefficients = -0.12, $P < 0.001$) and atmospheric temperature (standardized coefficients = -0.37, $P < 0.001$) had negative effects on moss growth. Moss (standardized coefficients = -0.98, $P < 0.001$) and biochar (standardized coefficients = -0.17, $P < 0.001$) had negative effects on soil evaporation.

Implications for and limitations to field situations

The prospect of applying moss colonization to hold water in karst lands is promising. Moss colonization could help to create supplementary approach during the high-cost afforestation in karst lands. The results of this study showed that growing moss significantly increased soil water holding capacity by reducing evaporation losses. In addition, as confirmed by the different slopes of the linear fitting equations, and the role of moss in reducing soil evaporation could be slightly enhanced by biochar application (Fig. 6 and 7). One of the most important findings in this study is that moss colonization could inhibit significantly surface crack development of carbonate-derived laterite (Fig. 3–5). This means that soil surfaces without moss colonization behave in completely different ways from those that retain them.

Our results shows that moss growth is not merely linear and irreversible, but that the moss can degrade after drying and recover after wetting. The relationship between moss growth and soil evaporation, therefore, fluctuates (Fig. 2). In Chen et al.'s (2018)

study, however, the model hypothesis was that moss coverage was always increasing and did not respond to natural disturbances (that is, dry–wet cycles). Therefore, the response of moss coverage to water stress should be considered in the eco-hydrology model to improve accuracy.

If moss colonization was used as a supplementary approach to afforestation in karst lands, the dynamic and ever-shifting relationships between moss growth and soil evaporation under dry–wet cycles should be emphasized. First, this study showed that moss growth was highly vulnerable to water deficits, especially in their early stages (Fig. 3). Therefore, the dampening effects of moss colonization on soil evaporation performed poorly with low coverage but worked well with high coverage (Fig. 7). A few previous studies have discussed the effects of biocrust with a high moss coverage (60% or 75%) on soil water movement (Berdugo et al., 2014; Zhao et al., 2014). However, moss coverage in this study was only up to 25%, due to cultivation time. It is also important that these findings be extended to other moss species. *Hypnum Hedw*., which was used in this study, might be unique, or it might represent a broader pattern among other moss species. Previous experiments and this study had ignored the moss transpiration due to the limitation of measurement method (Table 1). More measurement method should be performed for distinguishing between evapotranspiration and soil evaporation in future research. In addition, the usage of moss colonization might be limited to the shallow soil, making it difficult to

557 contribute significantly to deep soil in rocky desertification land (Xiao et al. 2014;
558 Chen et al. 2019; Liu et al. 2020).

559 **Conclusions**

560 The effects of moss colonization and biochar application on the evaporation
561 processes of carbonate-derived laterite were studied using four moss spore amounts (0,
562 30, 60, and 90 $g \cdot m^{-2}$) and four biochar application levels (0, 100, 400, and 700 $g \cdot m^{-3}$)
563 during six dry–wet cycles. The following results regarding the effects of moss
564 colonization and biochar application were obtained: 1) The increase of initial amount
565 of moss spores promotes the growth of moss (pr = 0.64), but biochar application
566 reduced slightly moss coverage (pr = -0.11); 2) Moss colonization decreased clearly
567 soil surface cracks (pr = -0.13), whereas biochar application had no distinguishable
568 influences on soil surface cracks ($P > 0.05$); 3) The relative cumulative evaporation
569 for the different biochar applications decreased with increasing moss coverage by
570 27.07%, 40.69%, 37.73%, and 31.37%, respectively. Biochar application reduced
571 critical moss coverage associated with inhibition of evaporation by 33.26%-44.34%; 4)
572 The mean surface temperature increased with an increase in the moss coverage (pr =
573 0.11); 5) A simplified empirical evaporation model could accurately estimate the
574 evaporation losses that were affected by the moss colonization and biochar
575 application, and the R^2 values ranged from 0.94 to 0.99.

576 These results suggested that moss colonization and biochar application played an
577 important role in evaporation processes in three primary ways. The artificially

578 cultivated moss, which was induced by moss spores and biochar, could decrease soil
579 evaporation by reducing soil surface cracks, increasing soil moisture and soil surface
580 temperature. It was concluded that the combination of moss colonization and small
581 amount biochar could be used as a supplementary approach to facilitate soil water
582 preservation in karst lands. However, there are still many questions to be answered in
583 future studies, including the role of moss colonization in the whole karst hydrology
584 (that is, infiltration, interception, runoff, and soil erosion).

Acknowledgments

We acknowledge and are grateful for the financial support provided by the National Natural Science Foundation of China through grant no. 41807016, the Guizhou Science and Talent Project ([2020]4Y010), the Science and Technology Funding of Guizhou Provincial Water Resources Department KT201803, the first class subject foundation of Guizhou Province (GNYL[2017]007) and the Guizhou Province Graduate Research Fund YJSCXJH[2020]094.

Conflict of interest

The authors declare that they have no known competing financial interests or personal relationships that could have appeared to influence the work reported in this paper.

References

Antoninka A, Bowker MA, Reed SC, Doherty K (2015) Production of greenhouse-grown biocrust mosses and associated cyanobacteria to rehabilitate dryland soil function. Rest Ecol 24:324-335

Berdugo M, Soliveres S, Maestre FT, (2014) Vascular plants and biocrusts modulate how abiotic factors affect wetting and drying events in dry lands. Ecosystems 17:1242-1256

Chamizo S, Cantón Y, Lázaro R, Domingo F (2013) The role of biological soil crusts in soil moisture dynamics in two semiarid ecosystems with contrasting soil textures. J Hydrol 489:74-84

Chamizo S, Cantón Y, Miralles I, Domingo F (2012) Biological soil crust development affects physicochemical characteristics of soil surface in semiarid ecosystems. Soil Biol Biochem 49:96-105

Chen K (2019) Evolution law of fissures of red clay slope under dry-wet cycles J Journal of Architecture and Civil Engineering. 36:52-61

Chen N, Wang X, Zhang Y, Yu K, Zhao C (2018) Ecohydrological effects of biological soil crust on the vegetation dynamics of restoration in a dryland ecosystem. J Hydrol 563:1068-1077

Ding YL, Zhou YC (2019) Study on the coupling relationship between slope-soil thickness and rock exposed ratio in small karst watershed. Chinese Journal of Soil Science 5:51-59

Felde VJMNL, Chamizo S, Felix-Henningsen P, Drahorad SL (2018) What stabilizes biological soil crusts in the Negev Desert? Plant soil 29:9-18.

Gao LQ ,Zhao YG, Qin NQ, Zhang GX, Yang K (2012) Impact of Biological Soil Crust on Soil Physical Properties in the Hilly Loess Plateau Region China. Journal of Natural Resources 27:1316-1326

Jiang ZY, Li XY, Wei JQ, Chen HY, Li ZC, Liu L, Hu X (2018) Contrasting surface soil hydrology regulated by biological and physical soil crusts for patchy grass in the high-altitude alpine steppe ecosystem. Geoderma 326:201-209

Kidron GJ, Vonshak A (2012) The use of microbiotic crusts as biomarkers for ponding subsurface flow and soil moisture content and duration. Geoderma 181:56-64

Kidron GJ, Tal SY (2012) The effect of biocrusts on evaporation from sand dunes in the Negev Desert. Geoderma 179 104-112.

Lei WJ, Zhou XY (2019) Influence of biochar on migration of pesticide degradation product trichloro pyridinol in soil. Transactions of the Chinese Society of Agricultural Engineering 35:173-180

Li D, Yang B, Gao Z, Sun LX (2021) The effects of biomass ash on soil evaporation and cracking. Arab J Geosc 14:1-11

Li B, Zhang Z (2009) Species diversity of mosses crust and the effect in karst rocky

635 desertification control. Carsologica Sinica 28:55-60
636 Li Y, Piao S, Li LZ, Chen A, Wang X, Ciais P, Wang K (2018) Divergent hydrological
637 response to large-scale afforestation and vegetation greening in China. J Sci Adv
638 4 https://doi.org/10.1126/sciadv.aar4182
639 Liu D, She D (2020) Combined effects of moss crusts and pine needles on
640 evaporation of carbonate-derived laterite from karst mountainous lands. J Hydrol
641 https://doi.org/10.1016/j.jhydrol.2020.124859
642 Liu M, Xu X, Wang D, Sun AY, Wang K (2016) Karst catchments exhibited higher
643 degradation stress from climate change than the non-karst catchments in
644 southwest China: An ecohydrological perspective. J Hydrol 535:173-180
645 Mager DM, Thomas AD (2011) Extracellular polysaccharides from cyanobacterial
646 soil crusts: a review of their role in dryland soil processes. J Arid Environ
647 75:91-97
648 Meng X, Yuan W (2014) Can biochar couple with algae to deal with desertification?
649 Journal of Sustainable Bioenergy Systems 4:194-198
650 Ni A, Chao ST, Shi KX, Xue PG, Bin S, Hilary II (2018) Effects of soil characteristics
651 on moisture evaporation. Eng Geol 239:126-135
652 Poulsen TG, Cai W, Garg A (2020) Water evaporation from cracked soil under moist
653 conditions as related to crack properties and near-surface wind speed. J Eur J
654 Soil Sci 71:627-640
655 Swaffer BA, Holland KL (2015) Comparing ecophysiological traits and
656 evapotranspiration of an invasive exotic Pinus halepensis in native woodland
657 overlying a karst aquifer. Ecohydrology 8:230-242
658 Tang CS, Cui YJ, Shi B, Tang AM, Liu C (2011) Desiccation and cracking behaviour
659 of clay layer from slurry state under wetting−drying cycles. Geoderma
660 166:111-118
661 Tang CS, Shi B, Liu C, Suo WB, Gao L (2011) Experimental characterization of
662 shrinkage and desiccation cracking in thin clay layer. Appl Clay Sci 52:69−77
663 Thomas SC, Frye S, Gale N, Garmon M, Launchbury R, Machado N, Melamed S,
664 Murray J, Petroff A, Winsborough C (2013) Biochar mitigates negative effects of
665 salt additions on two herbaceous plant species. J Environ Manage 129:62-68
666 Wan Y, Wu C, Xue Q, Hui X (2019) Effects of plastic contamination on water
667 evaporation and desiccation cracking in soil. Sci Total Environ 654:576-582
668 Wang C, Zhang ZY, Liu Y, Fan SM (2017) Geometric and fractal analysis of dynamic
669 cracking patterns subjected to wetting-drying cycles. Soil Till Res 170:1-13
670 Wang T, Stewart CE, Sun C, Wang Y, Zheng J (2018) Effects of biochar addition on
671 evaporation in the five typical Loess Plateau soils. Catena 162:29-39
672 Wang QX, Ju MC, Bu CF (2019) Effects of bacillus and a plant growth regulator for
673 provenance propagation of moss biocrusts. Bulletin of Soil and Water
674 Conservation 39:166-171
675 Wei ML, Zhang YM (2010) Effects of dehydration on photosynthetic pigment content

676 and chloroplast ultrastructure of syntrichia caninervis in biological soil crusts.
677 Journal of Desert Research 30:1311-1318
678 Wu K, Darcet D, Wang Q, Sornette D, (2020) Generalized logistic growth modeling
679 of the COVID-19 outbreak in 29 provinces in China and in the rest of the world.
680 Xiao B, Hu K, Ren T, Li B (2016) Moss-dominated biological soil crusts significantly
681 influence soil moisture and temperature regimes in semiarid ecosystems.
682 Geoderma 263:35-46
683 Xiao B, Sun F, Hu K, Kidron GJ (2019) Biocrusts reduce surface soil infiltrability and
684 impede soil water infiltration under tension and ponding conditions in dryland
685 ecosystem. J Hydrol 568:792-802
686 Xiao B, Wang QH, Zhao YG, Shao MA (2011) Artificial culture of biological soil
687 crusts and its effects on overland flow and infiltration under simulated rainfall.
688 Appl Soil Ecol 48:11-17
689 Xiao B, Zhao YG, Shao MA (2010) Characteristics and numeric simulation of soil
690 evaporation in biological soil crusts. J Arid Environ 74:121-130
691 Xiao B, Zhao Y, Wang Q, Li C (2015) Development of artificial moss-dominated
692 biological soil crusts and their effects on runoff and soil water content in a
693 semi-arid environment. J Arid Environ 117:75-83.
694 Xiao H, Xiong K, Zhang H, Zhang Q (2014) Research progress for karst rocky
695 desertification control models China. Population Resources and Environment
696 163:330-334
697 Xie SQ, Gao LQ, Zhao YG, Guo YW (2019) Responses of runoff and soil loss from
698 biological soil crustal slope to rainfall intensity under simulated rainfall. Chinese
699 Journal of Applied Ecology 30:391-397
700 Yang J, Xu X, Liu M, Xu C, Zhang Y, Luo W, Zhang R, Lia X, Kiely G, Wang K
701 (2017) Effects of “Grain for Green” program on soil hydrologic functions in
702 karst landscapes southwestern China. Agr Ecosyst Environ 247:120-129
703 Yang YS, Bu CF, Gao GX (2012) Effect of biological soil crust on soil temperature in
704 the Mu Us sand land. Arid Zone Res 29 352-359
705 Zhang J, Qun CHEN, Changfu YOU (2016) Biochar effect on water evaporation and
706 hydraulic conductivity in sandy soil. Pedosphere 26:265-272
707 Zhang R, Xu X, Liu M, Zhang Y, Xu C, Yi R, Luo W (2018) Comparing
708 evapotranspiration characteristics and environmental controls for three
709 agroforestry ecosystems in a subtropical humid karst area. J Hydrol
710 563:1042-1050
711 Zhang Y, Gu K, Li J, Tang C, Shen Z, Shi B (2020) Effect of biochar on desiccation
712 cracking characteristics of clayey soils. Geoderma 364
713 Zhao Y, Zhu Q, Li P, Zhao L, Wang L, Zheng X, Ma H (2014) Effects of artificially
714 cultivated biological soil crusts on soil nutrients and biological activities in the
715 Loess Plateau. J Arid Land 6:742-752
716 Zhou B, An H (2012) Research on problem of water resources security in guizhou and
717 its strategic solutions. Research of Agricultural Modernization 33:19-24
718 Zong Y, Chen D, Lu S (2014) Impact of biochars on swell-shrinkage behavior

719 mechanical strength and surface cracking of clayey soil. J Plant Nutr Soil Sci
720 177:920-926

721 **Table 1** Summary of previous studies contact with the effects of different types additive (organic and inorganic) in shallow soil on evaporation
722 processes, surface cracks and soil temperature.

Reference	Types of additives	Experimental designs	Scale	Soil thickness	Experimental methods	Effect on			Soil
						Evaporation	Soil surface crack	Soil temperature	
Li et al., 2021	Biomass ash	Open plexiglass container	4 cm height × 18 cm diameter	4 cm	1) Automatic weighing and photographing system investigated soil evaporation and crack 2) Digital image processing technology to identify crack	Evaporation might be decreased by increased resistance of water migration in soil	Biomass ash can effectively reduce soil surface crack	/	Clay
Zhang et al., 2020	Biochar	Square plexiglass container	20 × 20 × 1 cm	1 cm	1) High-precision (0.01g) electronic balance record the evaporation 2) High-definition camera + Digital image processing software (NJU-CIAS) analysis surface crack	Evaporation rate and duration in whole dry process was altered by increased soil porosity	Soil surface crack was inhibited by biochar of occupying soil shrinkage space	/	Clay
Wang et al., 2019	Plastic film	Copper tray	3 cm height × 22 cm	3 cm	1) Oven at 60°C measure soil water	Plastic film in soil might form covers to	Plastic film in soil strengthens	/	Clay

			diameter		content 2) High-definition camera + Digital image processing technology (Matlab 2010b) inspect surface crack	inhibit soil evaporation	surface crack		
Jiang et al ., 2018	Biocrust	PVC cylinder	6 cm height × 6 cm diameter	6cm	High-precision (0.01g) electronic balance record the evaporation	Biological crusts reduced soil evaporation by maintaining a lower soil temperature	/	Biocrusts reduced the soil surface temperature	Silt-loam
Ni et al., 2018	Quartzite	Cylindrical evaporator	0.7, 1.4, 2.1 and 2.8 cm height × 6.18 cm diameter	0.7-2.8 cm	1) High-precision electronic balance record the evaporation 2) WP4 method set out soil water retention curves	Larger soil thicknesses extend the constant evaporation rate stage	/	/	Clay
Wang et al., 2018	Biochar	PVC cylinder	10 cm height × 10 cm diameter	10 cm	High-precision (0.01g) electronic balance record the evaporation	Biochar had opposite effects in two evaporation stages (constant rate and falling rate stage)	/	/	Loess, Sand
Zribi et al., 2015	Plastic, pine bark and wheat	Square copper tray and microlysimeters	29 cm × 19 cm × 5 cm 10 cm	5 cm 10 cm	High-precision (0.01g) electronic balance record the evaporation	Effect of mulching material on evaporation depended on	/	/	Clay

	straw		height × 7.6 cm diameter			meteorological and experimental conditions and evaporation stage			
Chamizo et a., 2012	Biocrust	Polyvinyl chloride microlysimeters	5 cm height × 10cm diameter	5 cm	1) Terrestrial laser scanner (Leica Scan Station 2) + software (SAGA 2.0.5) investigate soil surface roughness 2) High-precision (0.01g) electronic balance record the evaporation	Effect of different biocrusts on soil evaporation was not significant in the case of low water content	/	/	Silt
Kidron et al., 2012	Biocrust	Petri dishes	1 cm height × 10cm diameter	10 cm	High-precision (0.01g) electronic balance record the evaporation	High-biomass biocrust could retain more water to decrease evaporation	/	Biocrust increased soil subsurface temperature	Sand
Xiao et al., 2010	Biocrust	PVC micro-lysimeters	15 cm height × 10cm diameter	15 cm	High-precision (0.01g) electronic balance record the evaporation	Effects of biocrust on evaporation were dependent on soil properties	/	Biocrust decreased soil surface temperature	

723 **Table 2** Basic properties of carbonate-derived laterite, moss spore and biochar used in
724 this study.

	Property	Unit	Value
Soil	Textural class	–	Silt loam
	Organic matter content	g kg^{-1}	51.60±0.33
	$EC_{1:5}$	us cm^{-1}	232.22±14.35
	Bulk density;	g cm^{-3}	1.28-1.35
	pH	-	5.56±0.15
	θ_0	g g^{-1}	0.15
	Clay (< 2 μm)	%	1.25±0.36
	Silt (2-50 μm)	%	77.48±0.51
	Sand (> 50 μm)	%	21.28±0.82
Moss spore	Main species	-	*Hypnum Hedw*
	Manufacturer	-	Cao Mu Ji Plant Research Center, China
Biochar	Main species	-	*Pinus sylvestris*
	Pyrolysis temperature	℃	450-550
	$EC_{1:5}$	us cm^{-1}	1149±31
	pH	-	10.32±0.03
	Manufacturer	-	Li Zhe Environmental Technology, China

725 Textural class based on the USDA classification, θ_0: initial gravimetric soil water
726 content, $EC_{1:5}$: soil electrical conductivity of a 1:5 soil-to-water extra.

Table 3 Equations for estimating growth of moss and soil evaporation loss.

Treatment	Moss spore ($g\ m^{-2}$)	Biochar application ($g\ m^{-3}$)	Fitting equation								
			Step:$Mc = \frac{M}{[1+be^{(-kt)}]}$					Step:$E_c = E_{c0}(aM_c + c)$			
			M	*b*	*k*	*RMSE*	R^2	*a*	*c*	*RMSE*	R^2
B0M1	30	0	0.11	22.72	0.07	0.04	0.66	-0.24	1.00	0.20	0.98
B0M2	60	0	0.09	19.85	0.07	0.04	0.61	-0.12	1.01	0.16	0.99
B0M3	90	0	0.17	21.78	0.09	0.16	0.60	-0.27	0.99	0.29	0.97
B1M1	30	100	0.07	23.71	0.07	0.02	0.69	0.14	0.94	0.43	0.94
B1M2	60	100	0.11	21.13	0.08	0.06	0.66	-0.17	1.02	0.25	0.98
B1M3	90	100	0.15	18.44	0.06	0.09	0.74	-0.50	0.98	0.38	0.95
B2M1	30	400	0.06	21.13	0.07	0.02	0.63	-0.14	0.97	0.38	0.96
B2M2	60	400	0.12	35.60	0.09	0.06	0.73	-0.09	1.01	0.29	0.97
B2M3	90	400	0.13	24.71	0.07	0.08	0.71	-0.43	1.02	0.34	0.97
B3M1	30	700	0.12	24.68	0.04	0.02	0.63	0.18	1.04	0.31	0.98
B3M2	60	700	0.10	20.88	0.08	0.05	0.60	0.52	1.01	0.29	0.98
B3M3	90	700	0.15	54.27	0.10	0.11	0.69	0.01	1.01	0.35	0.96

E_{c0}: evaporation of bare soil; *Ec*: daily evaporation of soil under different moss cover; SWC_{mean}: mean gravimetric soil water content; *Mc*: moss coverage; *M*: maximum moss coverage after growth; *b*: time for mutation of growth rate; *k*: growth rate corresponding to maximum moss coverage; *t*: growth time; *a* and *c*: evapotranspiration empirical coefficients considering mossy and biochar effects.

731 **Table 4** Partial correlations between soil evaporation and environmental factors.

Partial correlation	M_c (%)	R_{cr}(%)	$T_{soil\ suface}$ (℃)	SWC_{mean}	E (mm day^{-1})
Biochar application (g cm^{-3})	-0.11**	-0.22	0.01	0.07	0.01
Moss spores (g m^{-2})	0.64**	-0.01	0.12*	0.03	0.11*
SWC_{mean} (g g^{-1})	0.48**	-0.58**	0.36**	/	0.12*
M_c (%)	/	-0.13*	0.11**	0.48**	-0.22**
R_{cr} (cm^2 cm^{-2})	-0.13*	/	0.19**	-0.37**	0.32**
T_{air} (℃)	-0.24**	0.34**	0.43**	-0.49**	0.42**
RH_{mean} (-)	-0.33**	-0.18**	-0.16**	-0.13**	0.09*

732 SWC_{mean}: mean soil water content at dry process; $T_{soil\ surface}$: mean soil surface
733 temperature in 12:00 (℃); T_{air}: mean air temperature (℃); RH_{mean}: mean atmospheric
734 relative humidity; M_c: coverage of moss (%); R_{cr}: mean soil surface crack ratio (%); E:
735 daily mean evaporation rate (mm day^{-1}); Significant at *P < 0.05, **P < 0.01.

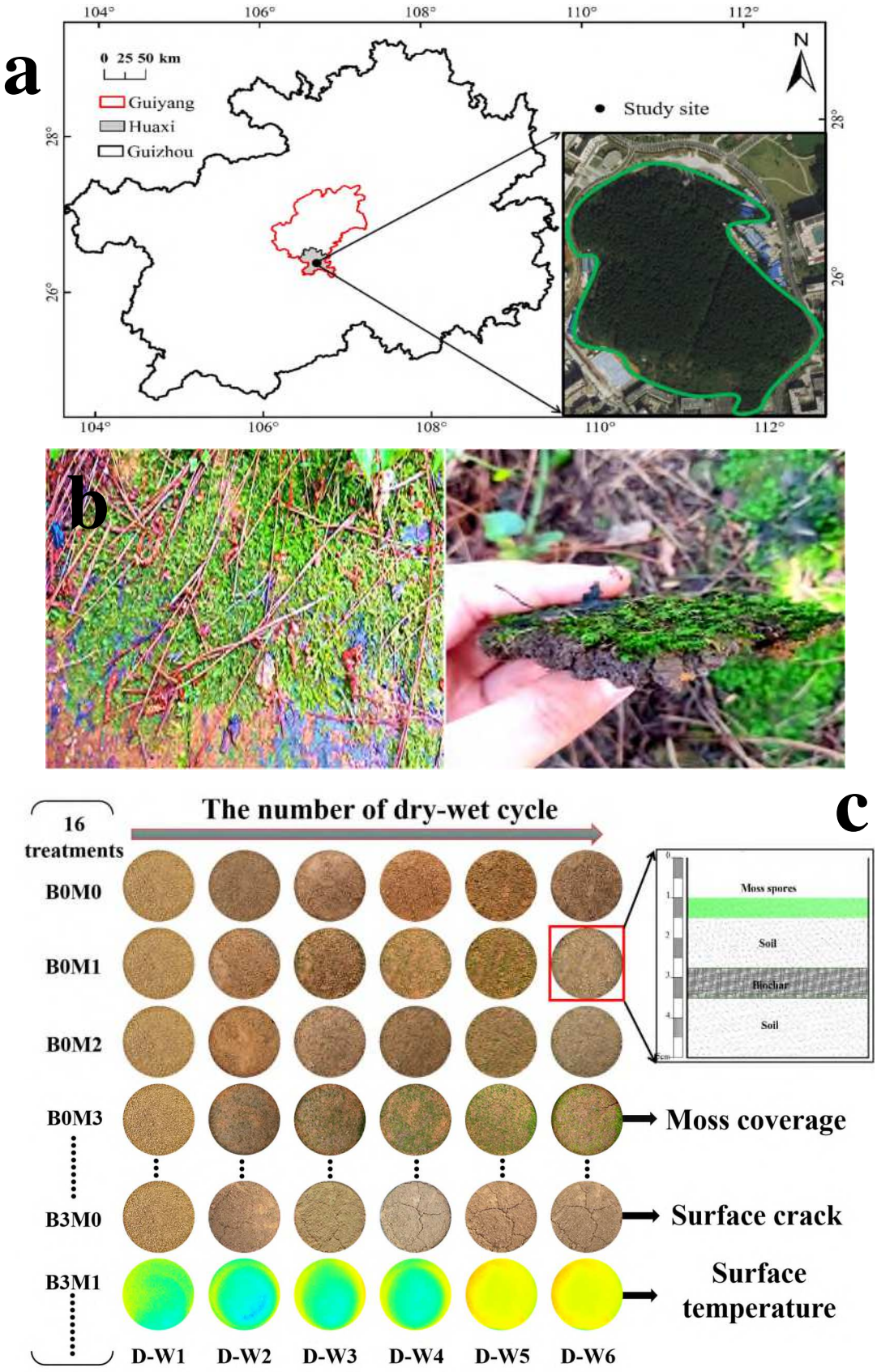

736 **Fig. 1** Soil collection site in Huaxi District, Guizhou Province, China (a), Landscape
737 covered by moss in karst mountainous lands (b), an evaporation experiment in
738 microlysimeter during six dry–wet cycles.

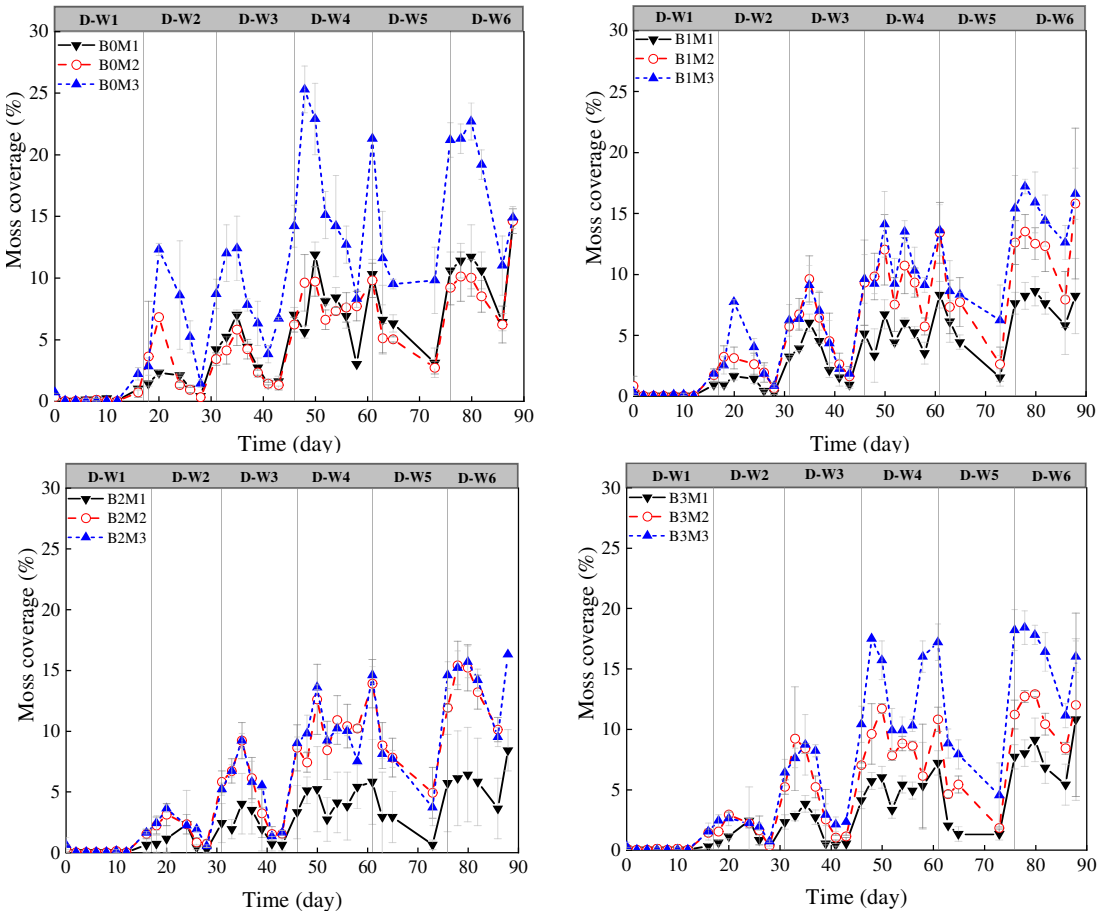

739 **Fig. 2** Moss coverage versus time for different amounts of biochar application (B0,
740 B1, B2 and B3) and moss spore (M1, M2 and M3) during six drying-wetting cycles.
741 D-W1, D-W2, D-W3, D-W4, D-W5 and D-W6 represent the first, second, third,
742 fourth, fifth, and sixth dry-wet cycle, respectively. Note that no growth of moss
743 occurred in M0 treatments.

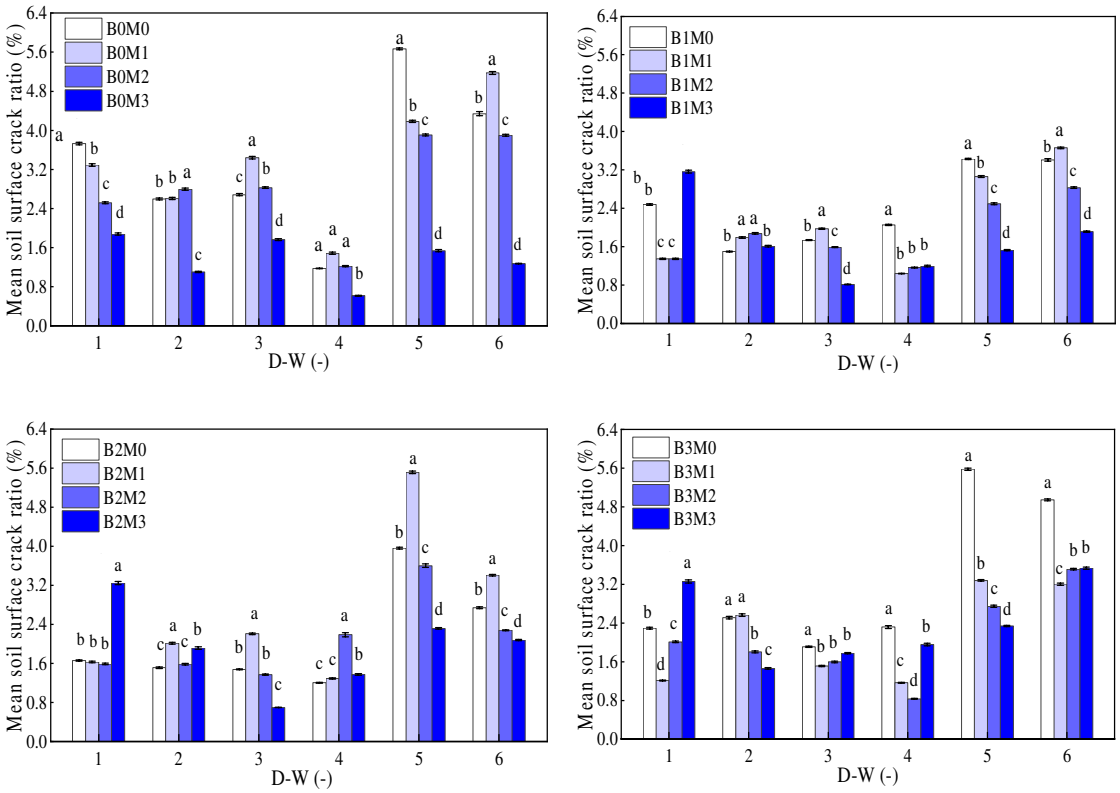

744 **Fig. 3** Mean soil surface crack ratio versus dry-wet cycle for different amounts of
745 moss spore (M0, M1, M2 and M3) and biochar application (B0, B1, B2 and B3).

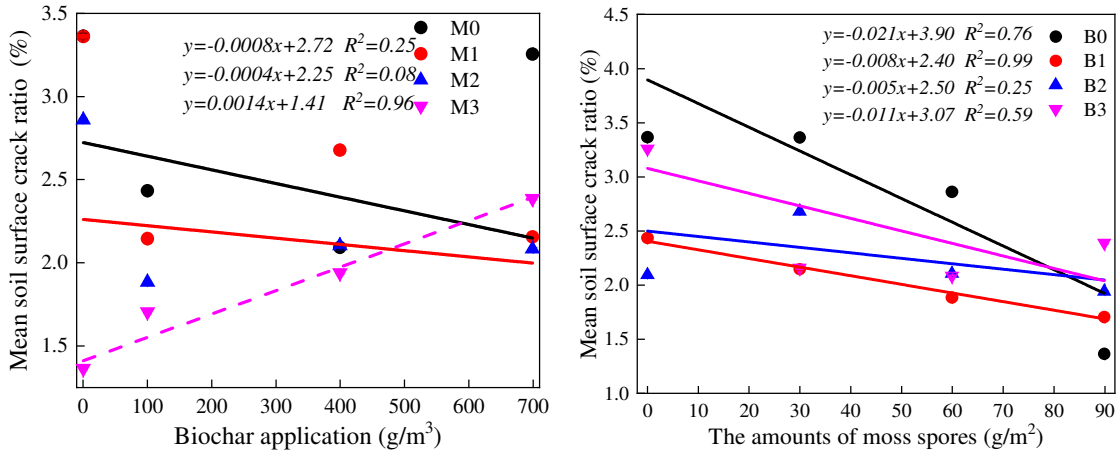

746 **Fig. 4** Mean soil surface crack ratio (R_{cr}) during the whole experimental duration for
747 different amounts of moss spore (M0, M1, M2 and M3) and biochar application (B0,
748 B1, B2 and B3).

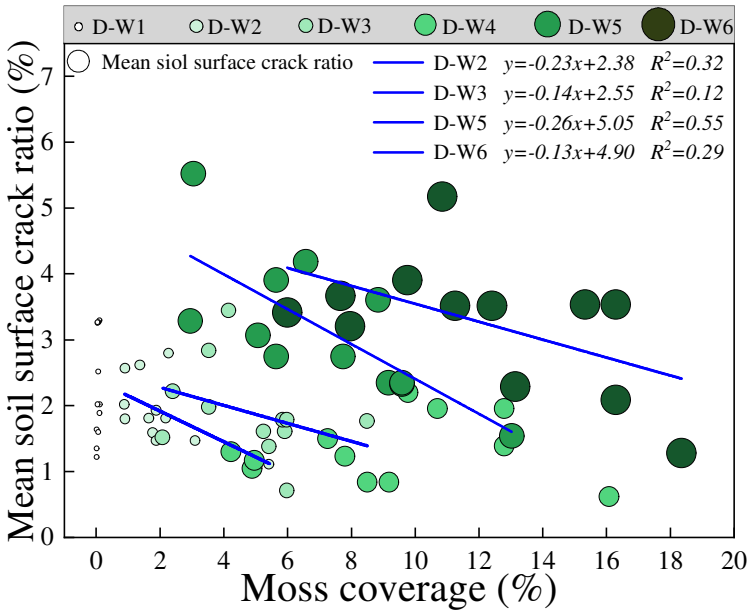

749 **Fig. 5** Relationships of mean soil surface crack ratio and moss coverage for each
750 dry-wet cycle.

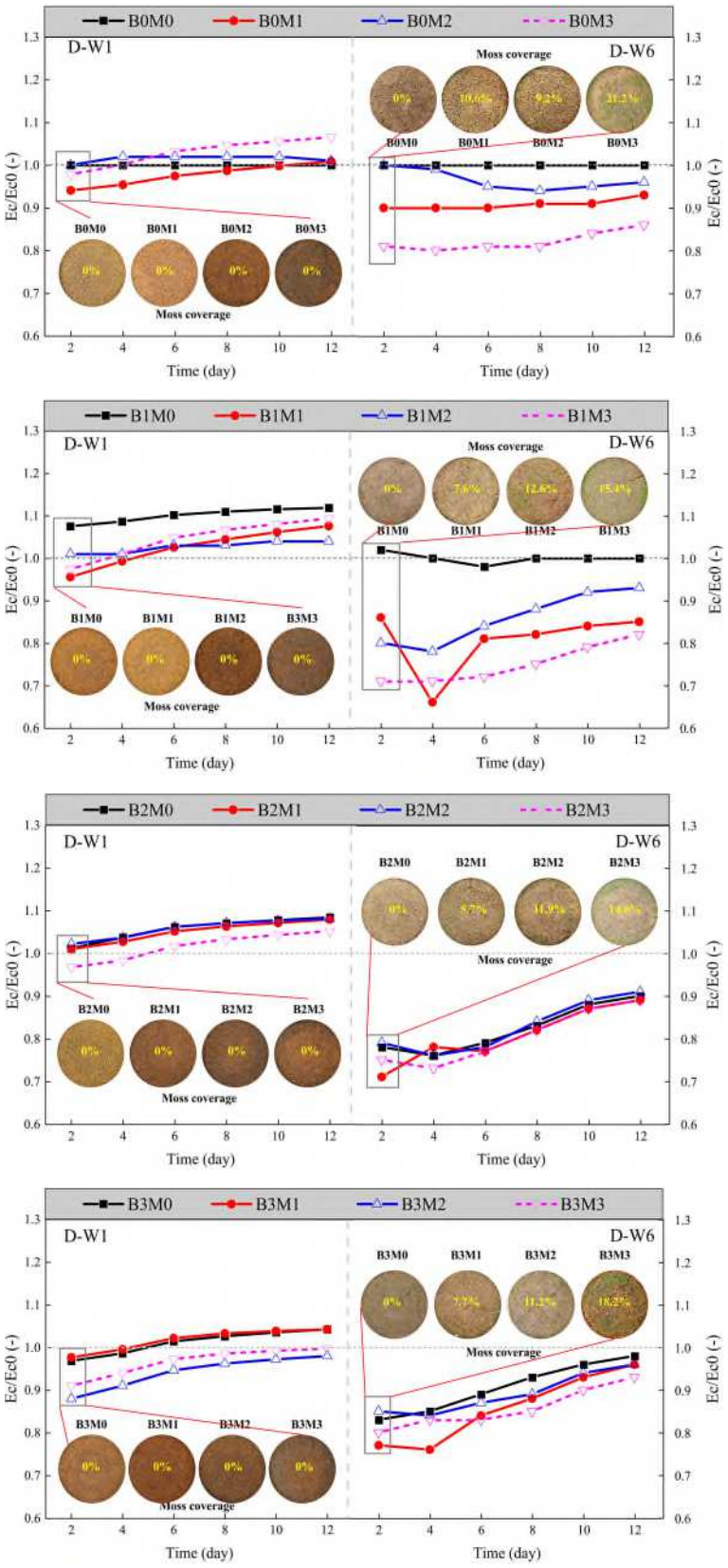

751

752

753

754

755 **Fig. 6** Relative cumulative evaporation (E_c/E_{c0}, -) versus evaporation time for
756 different amounts of moss spores (M0, M1, M2 and M3) and biochar applications (B0,
757 B1, B2 and B3) during D-W1 and D-W6. Relative cumulative evaporation (E_c/E_{c0}, -)
758 was calculated as the ratio of cumulative soil evaporation (E_c, mm) for all treatments
759 to cumulative bare evaporation (E_{c0}, mm) for B0M0 treatment

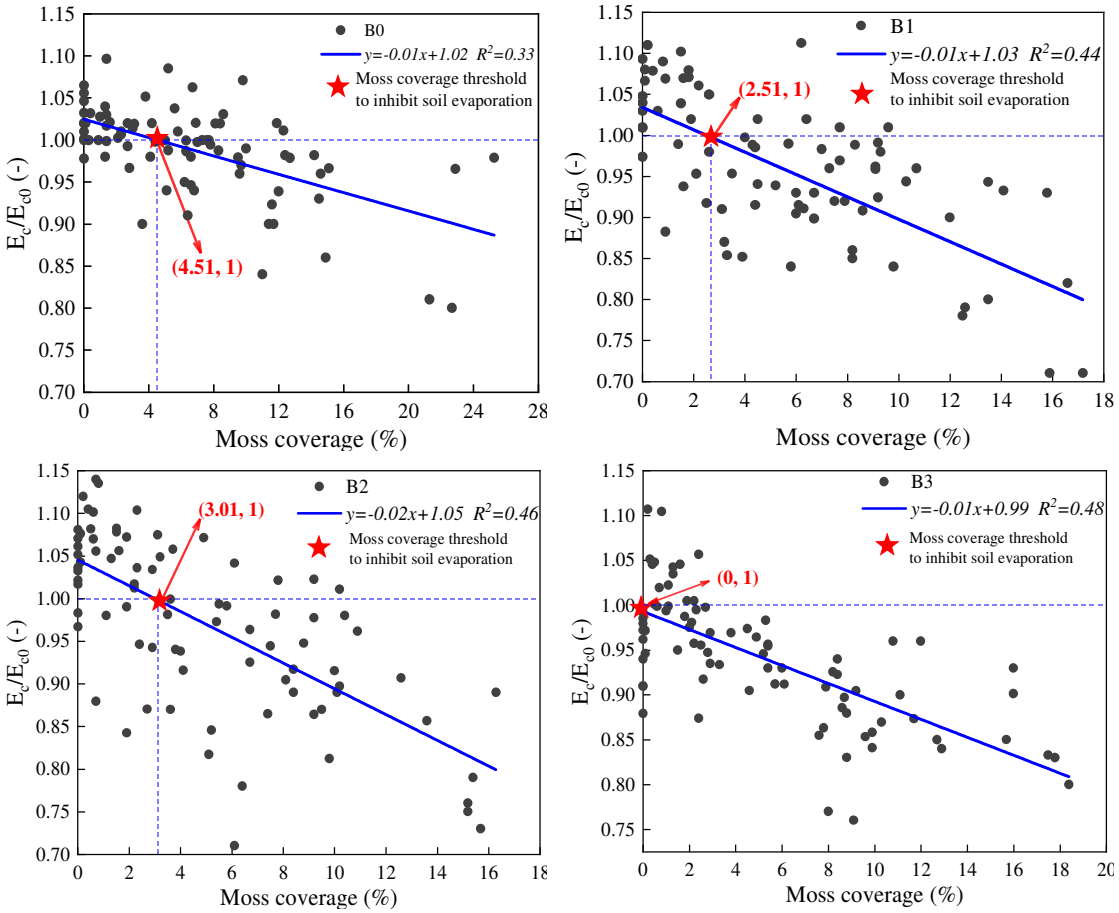

Fig. 7 Relative cumulative evaporation (E_c/E_{c0}, -) versus moss coverage (%) for different biochar applications (B0, B1, B2 and B3) for all six dry-wet cycles. Relative cumulative evaporation (E_c/E_{c0}, -) was calculated as the ratio of cumulative soil evaporation (E_c, mm) for all treatments to cumulative bare evaporation (E_{c0}, mm) for B0M0 treatment.

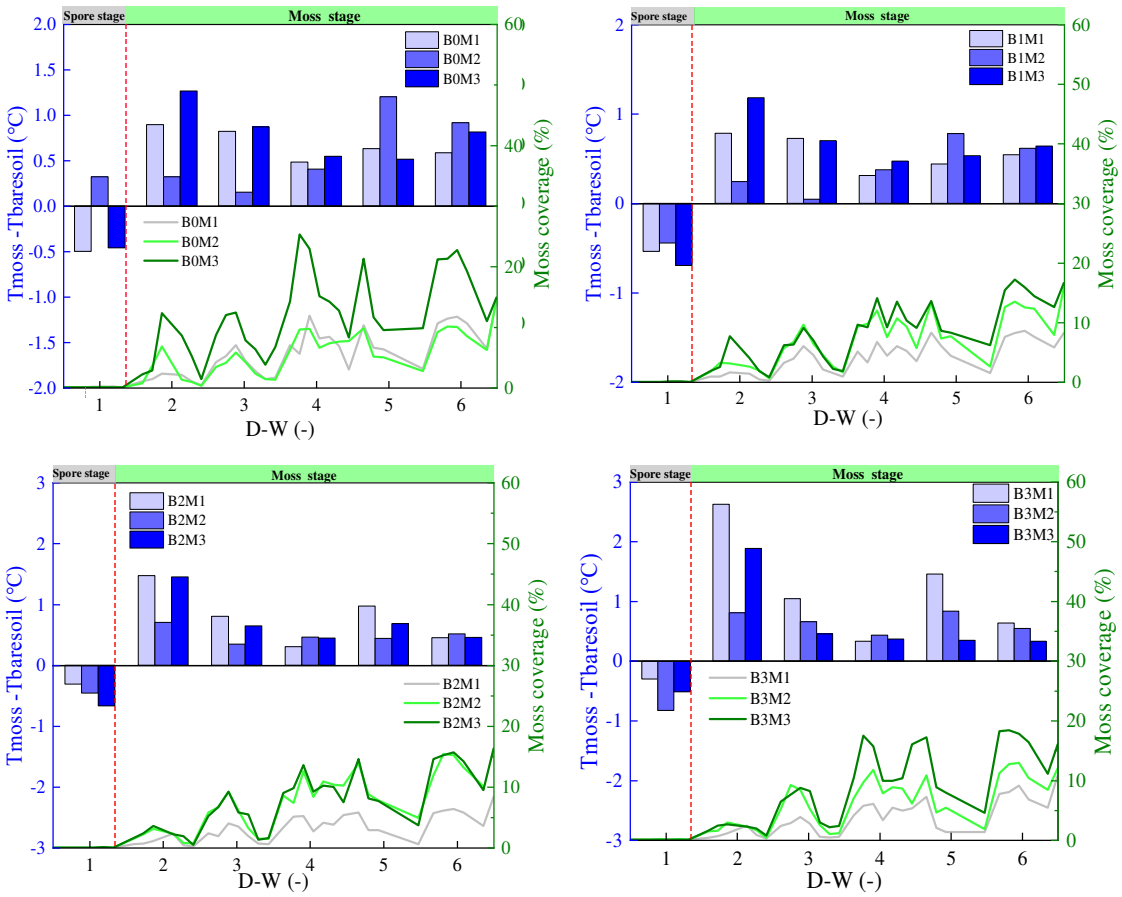

765 **Fig. 8** Difference between Soil surface temperature with moss and bare soil
766 temperature (T_{moss} - $T_{bare\text{-}soil}$) at 12:00 versus moss spores for different biochar
767 applications (B0, B1, B2 and B3) during the all dry-wet cycles.

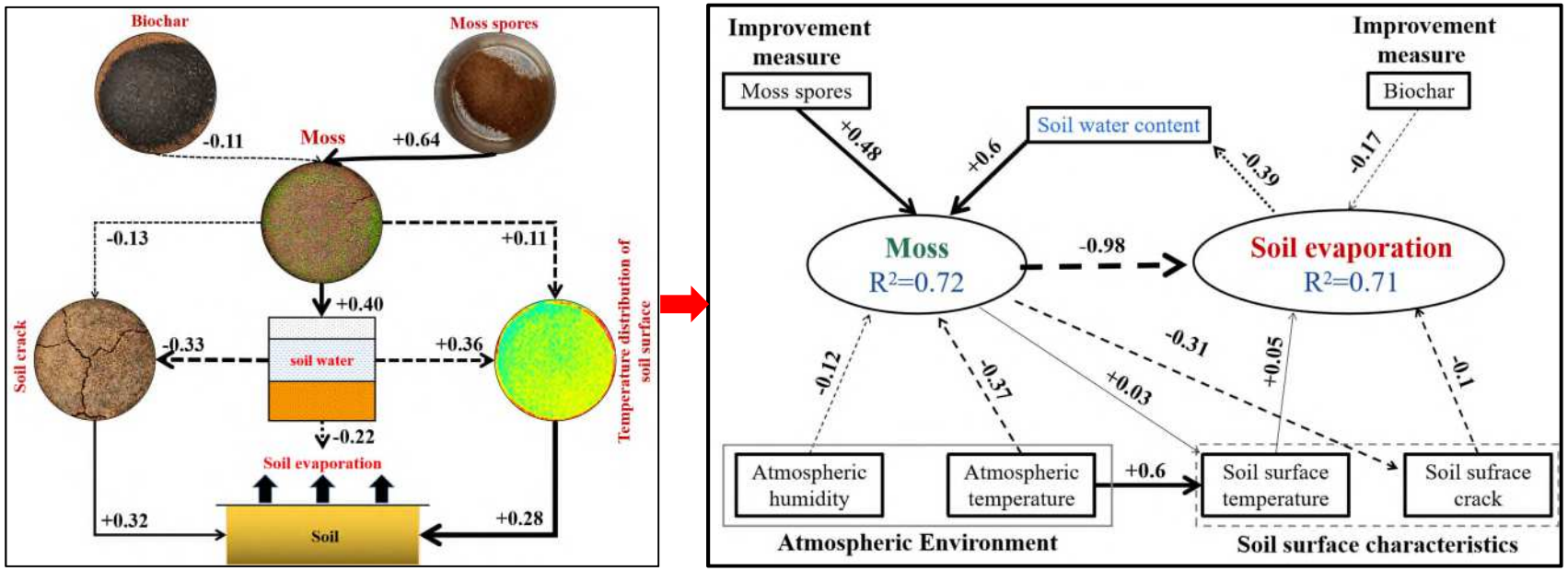

768 **Fig. 9** Schematic or mind map about the effects of initial moss spores amounts, moss coverage and biochar application on soil evaporation
769 processes of carbonate-derived laterite during dry-wet cycles. Numbers adjacent to arrows are standardized path coefficients of the relationship.
770 R^2 = the proportion of variance explained. P values are as follows: * < 0.05; ** < 0.01; *** < 0.001. Blue and red lines are positive and negative
771 relationships, respectively.

Supplementary Files

This is a list of supplementary files associated with this preprint. Click to download.

- Supplementarydata2021.11.23.docx